International Journal of Coal Geology 185 (2018) 103–118

Contents lists available at ScienceDirect

International Journal of Coal Geology

journal homepage: www.elsevier.com/locate/coal

Raman spectroscopy to study thermal maturity and elastic modulus of kerogen

Seyedalireza Khatibi[a,*], Mehdi Ostadhassan[a], David Tuschel[b], Thomas Gentzis[c], Bailey Bubach[a], Humberto Carvajal-Ortiz[c]

[a] University of North Dakota, Grand Forks, ND 58203, United States
[b] HORIBA Scientific, 3880, Park Avenue, Edison, NJ 08820, United States
[c] Core Laboratories, 6316 Windfern Road, Houston, TX 77040, United States

ARTICLE INFO

Keywords:
Kerogen
Raman spectroscopy
PeakForce AFM
Elastic modulus

ABSTRACT

Although organic-rich oil-producing mudrocks have been studied extensively during the last decade, kerogen, as one the main constituents, is not thoroughly understood. The unknowns about kerogen elevate when it comes to its modulus of elasticity. Since kerogen is not as stiff as inorganic minerals, its presence can have a significant impact on the initiation and propagation of fractures in kerogen-rich formations that should undergo stimulation.

This study proposes an approach to estimate modulus of elasticity of kerogen with different thermal maturities using Raman spectroscopy. Various shale samples from the upper and lower members of the Bakken Formation were picked from several wells within the Williston Basin in North Dakota, USA. These samples were analyzed using Rock-Eval (RE) pyrolysis and vitrinite reflectance (%Ro) for thermal maturity. In addition, Raman spectroscopic measurements were made on samples and followed by PeakForce AFM for Young's modulus estimation of the organic matter. First, the Raman responses were correlated with the thermal maturity and then, a correlation was established to show the potential relationship between elastic modulus of organic matter and its Raman response based on the maturity levels.

1. Introduction

Organic matter, predominantly kerogen that has formed from the burial and preservation of living organisms, is interspersed within the mineral matrix (Hutton et al., 1994). Shale reservoirs with organic-rich intervals are often characterized by high quantities of kerogen, solid bitumen and also moveable hydrocarbons, which can be extracted through hydraulic fracturing and other stimulation methods.

Interest in the experimental and theoretical investigation of the mechanical properties of shale reservoirs has grown significantly in recent years due to the dependence of fracturing models on mechanical properties. Aoudia et al. (2010) and Kumar et al. (2012) presented how increasing total organic carbon (TOC) is correlated with a decrease in Young's modulus of shale, Fig. 1. Hu et al. (2015) concluded that shales with higher TOC have lower fracture pressure gradients. This implies that organic matter such as kerogen has a non-negligible effect on the overall rock mechanical response (Dietrich, 2015). Thus considering matrix mechanical properties along with an accurate knowledge of the TOC content, maturity, and mechanical properties of kerogen become important for a successful stimulation project.

TOC can be obtained from the Rock-Eval (RE) or LECO tests (Espitalie et al., 1985; Peters, 1986). Vitrinite reflectance (%VRo) is considered as one of the most reliable methods to obtain thermal maturity (Diessel et al., 1978). However, vitrinite reflectance can be challenging when samples contain very little or no primary vitrinite (Hackley et al., 2015; Sauerer et al., 2017).

In addition to RE and vitrinite reflectance, Raman spectroscopy can also provide us with valuable information regarding kerogen properties. Wopenka and Pasteris (1993) used laser Raman microprobe for characterizing the structural state of carbonaceous materials such as kerogen and coals (Zhao and Wagner, 2004). Kelemen and Fang (2001) studied kerogen and coals from various sources and established a correlation between Raman spectroscopy and maturity. Tuschel (2013) discussed the use of Raman spectroscopy for characterizing oil shales and showed the contribution of other materials such as calcite in the Raman spectrum. Other researchers have successfully used Raman spectroscopy as a powerful non-destructive tool to quantitatively evaluate thermal maturity of organic matter (Beyssac et al., 2002;

* Corresponding author.
E-mail address: Seyedalireza.Khatibi@und.edu (S. Khatibi).

https://doi.org/10.1016/j.coal.2017.11.008
Received 8 September 2017; Received in revised form 4 November 2017; Accepted 4 November 2017
Available online 07 November 2017
0166-5162/

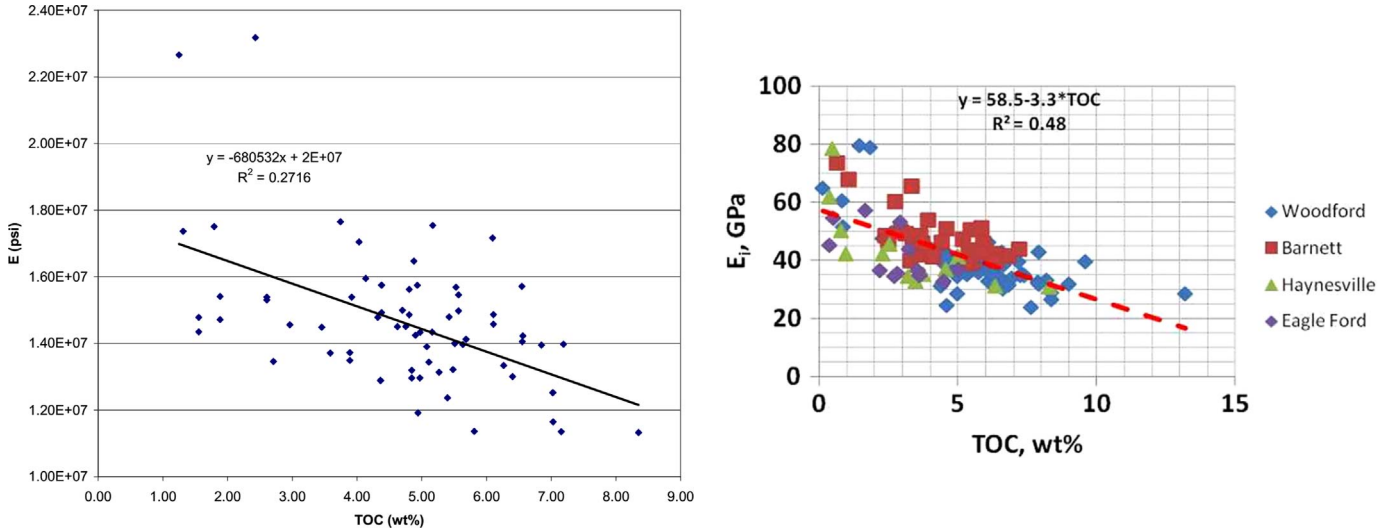

Fig. 1. Young's modulus of shale vs. TOC for: (left) the Woodford Shale formation, (right) the Woodford, Barnett, Haynesville and Eagle Ford Shale formations. Sources: From Aoudia et al., 2010 and Kumar et al., 2012, respectively.

Quirico et al., 2005; Lahfid et al., 2010; Guedes et al., 2012; Hinrichs et al., 2014; Wilkins et al., 2014; Zhou et al., 2014; Lünsdorf, 2016; Mumm and İnan, 2016; Ferralis et al., 2016). During thermal maturation, organic matter experiences an increase in aromaticity and a reduction in H, O, N and S content (Tissot and Welte, 1984). Such processes result in a more ordered-structure kerogen (Tyson, 1995; Waples, 1981), which allows Raman spectroscopy to detect different levels of maturation, reflecting these structural changes.

There has been a significant amount of research regarding the thermal maturity of kerogen, whereas its mechanical properties have not well studied (Manjunath and Nair, 2015). The reason for the minimal studies on mechanical properties of kerogen is mostly due to the lack of advanced equipment. Generally, to acquire mechanical properties of a sample in the lab, unconfined compressive strength (UCS) or tri-axial tests are performed on inch-sized cylindrical cores (Shukla et al., 2013; Alexeyev et al., 2017; Aghajanpour et al., 2017). While, kerogen is dispersed within the matrix, isolating a location that contains solely kerogen would be challenging. Thus, high-resolution equipment to study small volumes is required (Zhao et al., 2002; Ulm et al., 2007; Sweers et al., 2011; Schön et al., 2011; Trtik et al., 2012; Ghanbari et al., 2015; Babaei et al., 2015; Babaei et al., 2017; Manjunath and Nair, 2017). Nanoindentation is a testing technique to indirectly determine mechanical properties of materials at the micro- and nano-scales. Researchers in petroleum engineering have applied the nanoindentation method to study shale properties (Kumar et al., 2012; Mason et al., 2014; Pal-Bathija et al., 2008; Liu and Ostadhassan, 2017). These studies have been mostly focused on the minerals and not the kerogen. A few studies investigated mechanical properties of kerogen with more advanced analytical equipment. Eliyahu et al. (2015) acquired atomic force microscopy (AFM) to examine mechanical properties of organic matter. Li et al. (2017) also used PeakForce AFM and measured the nanomechanical properties of kerogen with high precision.

In this study, first, Raman spectroscopy was used to detect the Raman spectrum of kerogen. Then, the mapping mode of AFM described by Li et al. (2017) was utilized to determine the Young's modulus of the organic particles within our samples. In the next step, a new approach was proposed to understand how the mechanical properties of kerogen in terms of Young's modulus could be reflected on the Raman spectra. It should be noted that the samples are also analyzed for thermal maturity to make this relationship more meaningful. This preliminary study will improve our understanding about the kerogen mechanical properties and will provide a fast, inexpensive and non-destructive method to estimate its modulus of elasticity.

2. Geological setting

For this study, samples were chosen from the upper and lower members of the Bakken Formation and analyzed with Raman, Rock-Eval, vitrinite reflectance and AFM PeakForce. The Bakken Formation is an organic rich shale, mudstone and sandstone that was deposited during the Late Devonian and Early Mississippian Periods. It is located in the Williston Basin, which is an elliptical shaped depression located in the western portion of North Dakota, northeastern region of Montana and extends into parts of Saskatchewan and Manitoba (Fig. 2) (Smith and Bustin, 2000).

The Bakken Formation is divided into three members, the Upper, Middle and Lower Bakken (Fig. 3). The upper and lower members are organic rich shales that were classified by Smith and Bustin (1995) as the same lithofacies. The lower member is composed of a finely laminated black mudstone. The black colour of the shale is due to the presence of organic matter in the rock, which can vary depending on the ratio of clay, silt, and carbonate in the rock (LeFever et al., 1991). Illite is the primary clay present and there is an abundance of authigenic pyrite (Smith and Bustin, 1995). The pyrite is present as lenses or nodules and it can also be found distributed throughout the shale members, occasionally filling in the fractures of the rock. The upper shale has a similar lithology to the lower shale, and varies in the amount of organic matter, as well as being more fossiliferous (LeFever et al., 1991).

The lower and upper members contain Type-I and Type-II organic matter that originated mostly from marine algae. The TOC has a maximum of 30% and 20% in the upper and lower members, respectively (Smith and Bustin, 1995). The organic matter is disseminated evenly throughout the lower member whereas the upper member has a higher amount of TOC.

The Middle Bakken overlies the Lower Bakken and is composed primarily of siltstones and sandstone. Smith and Bustin (1995) classified it as eight different lithofacies, and three different sub-units at a larger scale. The three sub-units are termed A, B, and C, with ascending depth respectively. The basal A sub-unit and upper C sub-unit are composed primarily of siltstone, with the middle sub-unit B having a composition of mud- and sandstone. The formation is massive and well sorted, due to bioturbation (LeFever et al., 1991). The Middle Bakken

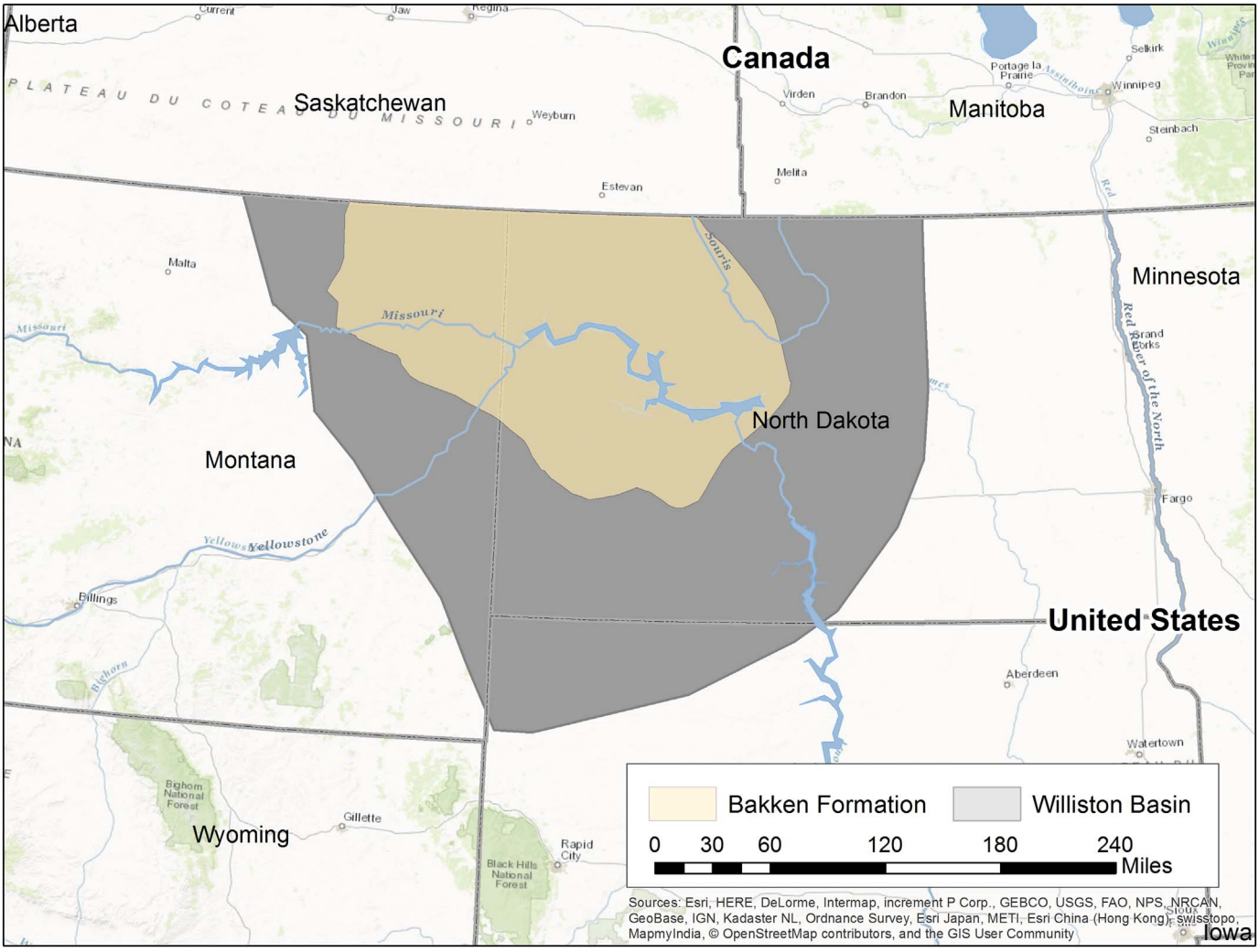

Fig. 2. Map of the Bakken Formation located in the United States portion of the Williston Basin. (Source: modified Liu et al., 2017).

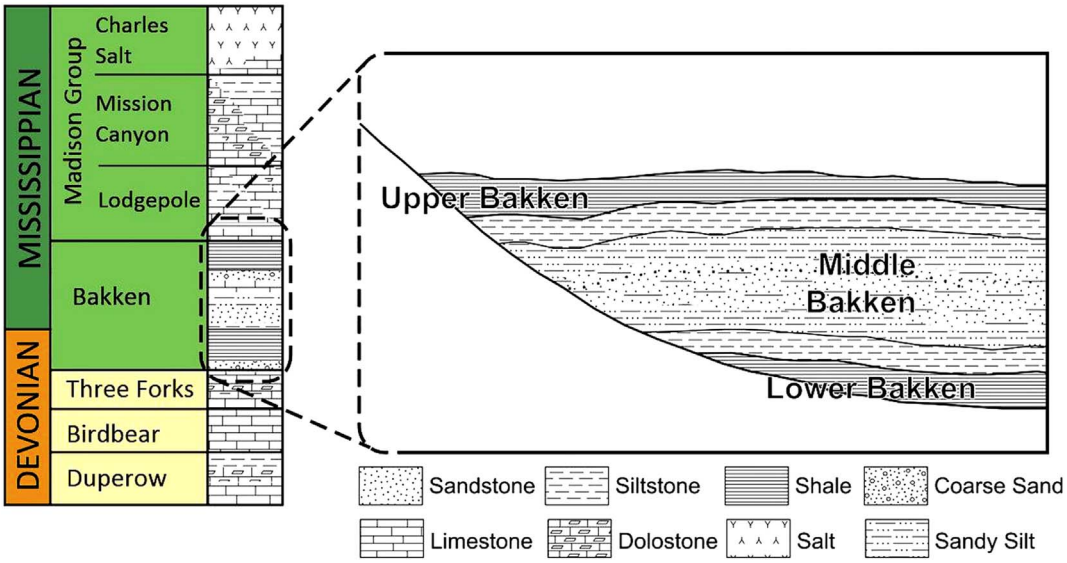

Fig. 3. Stratigraphic column representing the Bakken Formation and the associated lithology with the Upper, Middle, and Lower Members of the Bakken Formation. Source: Modified from Kuhn et al., 2010.

makes up < 0.1% TOC on average for the whole formation and is primarily targeted as a reservoir rock (Smith and Bustin, 1995).

Deposition of the formation began during the Upper Kaskaskia Sequence, during the Late Devonian Period. The Bakken Formation is recognized as the basal unit of the Upper Kaskaskia and is distinguishable by its black colour, as well as a sharp erosional contact with underlying Three Forks Formation. This unconformity is due to the rapid transgression that occurred at the start of the Upper Kaskaskia Sequence, leading to the deep marine depositional environment of the Lower Member of the Bakken Formation (Gerhard et al., 1990). The upper and lower shales were deposited in similar environments, which was conducive to an anaerobic environment that would preserve the organic matter. This occurred due to the depth of the water (> 200 m) being so large, that the point of deposition was below storm wave base, creating a stratified water column. The stagnant bottom water conditions, lead to an anoxic environment containing a high concentration of hydrogen sulfide (Smith and Bustin, 1995). The Middle Bakken was deposited in three different episodes that range from offshore for sub-unit A, fair weather wave base and the zone of breaking waves for sub-unit B, and between storm and fair-weather wave base for sub-unit C (Smith and Bustin, 1995).

3. Samples and experiments

The samples were retrieved from six different wells varying in depth and maturities. Figs. 4 and 5, indicate well locations and the samples that were used for the experiments. Vitrinite maturity (%VRo) and Rock-Eval (RE) Pyrolysis measurements were carried out on the samples. RE is one of the most common methods for evaluating origin and thermal properties of kerogen by heating the samples in the absence of oxygen (Espitalie et al., 1985; Peters, 1986; Cheshire et al., 2017). Using the parameters that were generated from the RE analysis, kerogen production potential can be identified. Rock-Eval analysis of the samples revealed that the kerogen is mainly Type II, either immature or in the oil window as shown in Fig. 6. TOC values vary from 13.26 wt% to 24.71 wt%, and %VRo maturity from 0.38 to 0.94. Table 1 shows a summary of organic matter properties. For vitrinite reflectance (%VRo) analysis, the whole-rock samples were crushed to 20 mesh (850um) particles, mixed with the epoxy resin and hardener (ratio of 2:1) and left to harden under vacuum conditions for 24 h (Gorbanenko and Ligouis, 2014; Hackley et al., 2015). The samples were polished to ensure the surface is scratch and relief free by using Buehler EcoMet/AutoMet 250 automated polishing equipment. A Carl Zeiss Axio Imager A2m microscope, equipped with a white light source and a UV light to analyze the random reflectance in oil (%VRo) and qualitative fluorescence, was used for reflectance measurements and visual kerogen analysis.

Approximately 60–70 mg per sample were used for Rock-Eval pyrolysis. The instrument is Rock-Eval 6 analyzer, commercialized by Vinci Technologies in France. The pyrolysis method was the Default method, in which the sample is placed in the chamber and heated at 300 °C isothermally for 3 min before the temperature is increased to 650 °C at a rate of 25 °C/min. The detailed Rock-Eval pyrolysis procedure and the parameters obtained from this analysis are outlined in Behar et al. (2001).

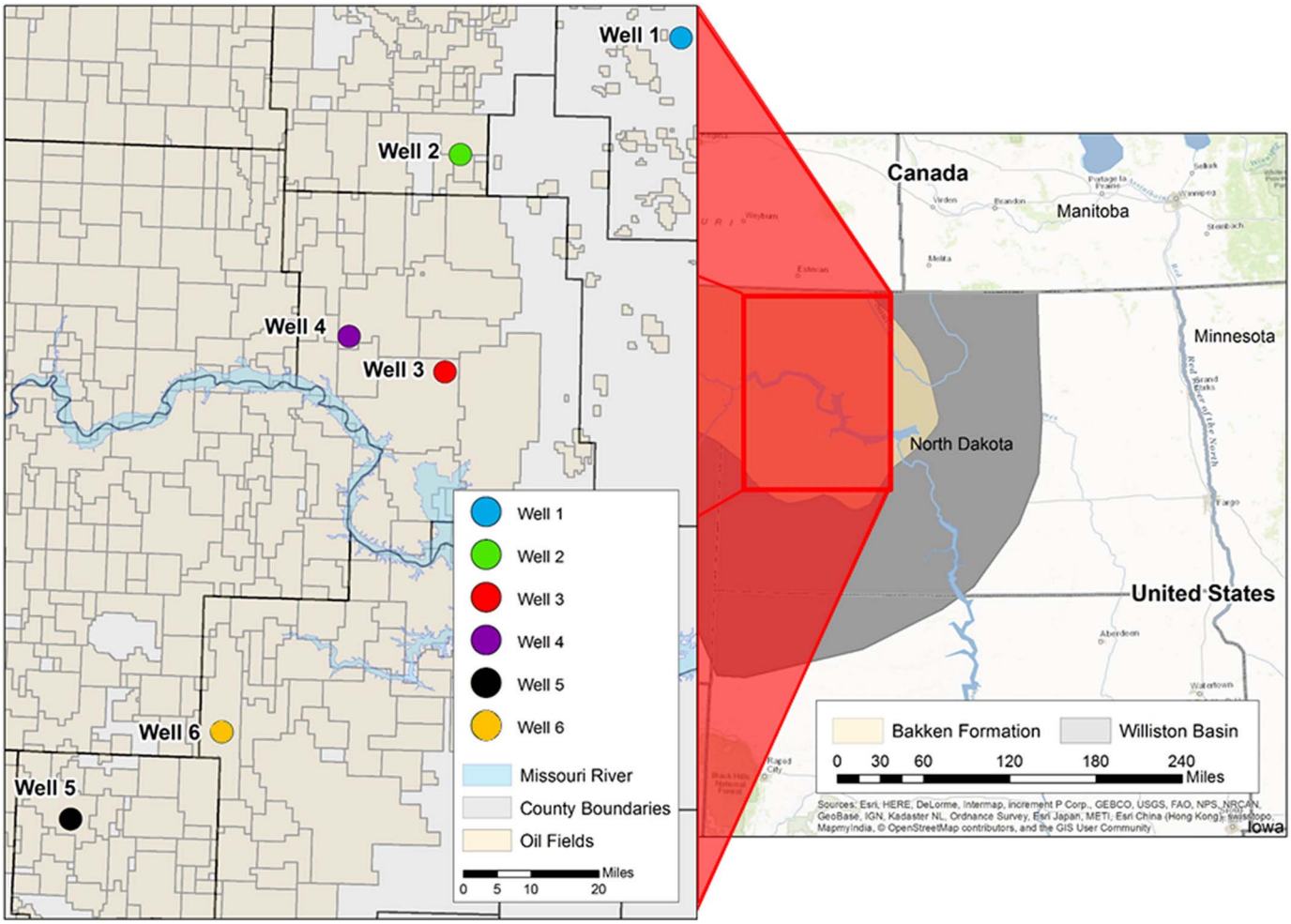

Fig. 4. Wells used in the study distributed throughout the Bakken Formation, Williston Basin, ND.

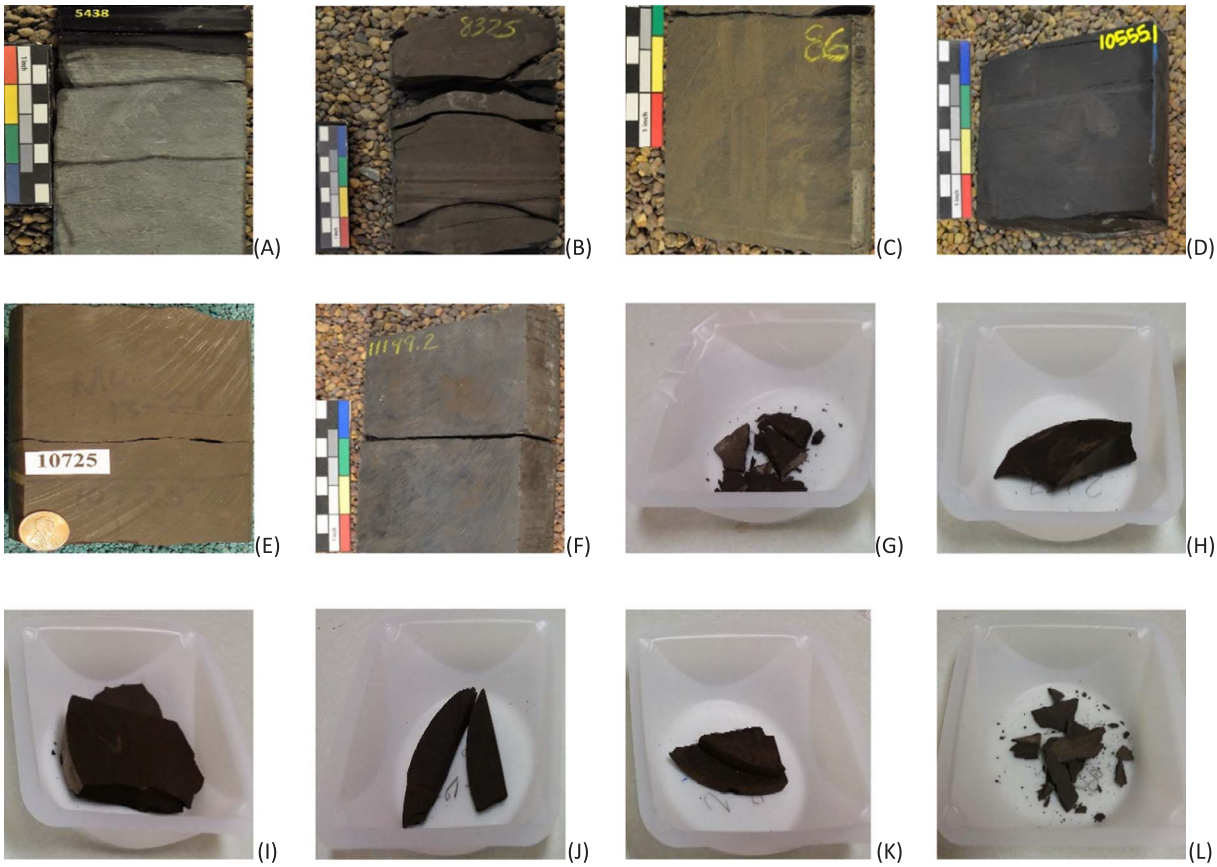

Fig. 5. (A) to (F) Photo of core samples of Well No.1 to 6, respectively. (G) to (L) corresponding sample chips for Raman measurements.

3.1. Raman spectroscopy

Raman scattering as a function of the molecular vibrations and symmetries of chemical bonds is a method to study carbon atoms. The first step in producing a Raman spectrum is to illuminate the sample with a monochromatic light source (Tuinstra and Koenig, 1970). This illumination causes a Raman shift, since photons (particles of light) exchange part of their energy with molecular vibrations in the material (Wang et al., 1990; Reich and Thomsen, 2004). The change in energy depends on the frequency of vibration of the molecule(s). Studies have been conducted to assess the structure of carbonaceous materials by utilizing Raman spectroscopy (Ferrari and Robertson, 2000; Reich and Thomsen, 2004; Keown et al., 2007; Ammar et al., 2015).

The Raman spectrum of kerogen consists of two main peaks known as G and D bands (Cesare and Maineri, 1999; Marshall et al., 2010; Tuschel, 2013). The G band refers to graphite, which appears at approximately 1600 cm^{-1} with a sharp peak. The origin of the G band is due to the inplane E_{2g2} vibrational modes of the carbon atoms in aromatic ring structures (sp^2 carbon) exhibiting $D_{6h}{}^4$ symmetry (Sauerer et al., 2017). The D band refers to a disorder in the atoms which appears around 1350 cm^{-1} as a narrow peak which is a result from the Raman-active A_{1g} symmetry associated with lattice defects and discontinuities of the sp^2 carbon network (Sauerer et al., 2017). During the process of maturity, kerogen endures aromaticity and tends to be more ordered which finally results in the disappearance of the disorder band. For poorly organized carbonaceous material, additional bands appear around 1150, 1350, 1500 and 1620 cm^{-1}. The significance and appearance of the minor bands are not well understood and strongly debated (Beyssac et al., 2003). In this study, major bands are considered.

Raman spectra for all samples in this study were acquired by focusing the laser beam on the surface of the samples where organic matter is detected with 532 nm excitation. The instrument was equipped with a 50 × long working distance optical microscope to easily locate the spot that Raman signals are going to be acquired. Scan range of the instrument was 100 μm × 100 μm with step size of 1 μm with the focal volume of around 3 μm^3. The high spatial resolution of the equipment enabled us to capture the Raman response of the organic matter with good accuracy. There is not any specific sample preparation such as polishing surfaces necessary. Grinding and polishing have shown to affect the lattice at the surface by creating additional defects, which causes Raman spectrum not to reflect the pristine sample signal (Lünsdorf, 2016).

Representative spectra for samples were obtained by acquiring spectrum from five locations on the surface of the samples, Fig. 7. The fluorescence background noise interferes with Raman signals, specifically with weaker signals (Kelemen and Fang, 2001). The background noise might be due to disordered organic matter, solid bitumen, residual mineral matter, diffuse presence of hydrogen, high sulfur content or generally low thermally mature samples (low mature samples are rich in N, S and O) (Tissot and Welte, 1984). Fig. 8 shows hydrogen-rich low-reflecting solid bitumen under white reflected and UV light (fluorescent). Note the dull-yellow fluoresce of the solid bitumen in Fig. 9, which can interfere with signals.

Producing a clear Raman spectrum from some samples was more challenging, such as Well No. 2 in which fluorescence background noise masked the Raman spectrum. In this case, a baseline subtraction processing method should be used to attenuate the noise, Fig. 9. This method allows the high background spectrum to be subtracted from the main spectrum and yields distinguishable bands. To do so, a curve was fitted mathematically through the baseline points on the background noise spectrum (red curve in Fig. 9) and then was subtracted from the main spectrum. Using this mathematical approach provides a flat zero baseline spectrum in order to pick band positions in a more straightforward manner. Mean of spectra for each sample was considered as

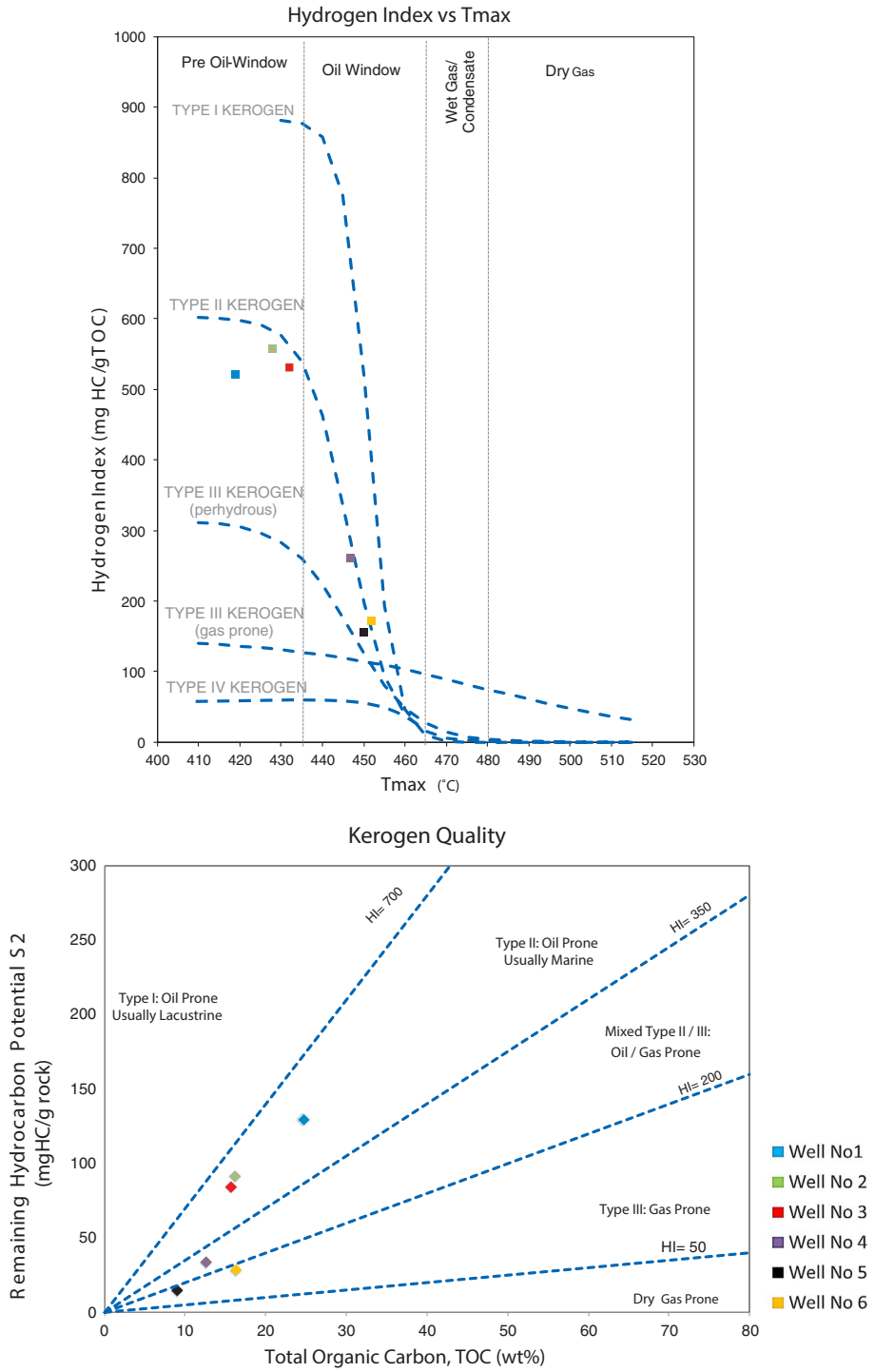

Fig. 6. Rock-Eval results showing Kerogen type based on HI vs. T_{max} (up) and S2 vs. TOC (down). As seen, samples are mainly Type II Kerogen.

Table 1
Properties of six samples used in this study from the Upper and Lower Bakken.

Well no.	Sample depth (ft)	TOC (wt%)	Ro (%)	S1	S2	HI	OI	T_{max} (°C)
1	5438	24.71	0.38	7.97	128.71	520.88	8.42	419
2	8326	16.27	0.54	8.27	90.69	557.41	2.15	428
3	9886	15.76	0.59	9.27	83.7	531.09	0.51	432
4	10,555	13.26	0.86	0.31	33.01	260.1	0.94	449
5	10,725.5	9.04	0.94	6.13	13.94	154.2	1.22	450
6	11,199	16.36	0.92	0.71	28.05	171.45	1.58	452

final spectrum, Fig. 10. Corresponding G and D bands characteristics are summarized in Table 2.

3.2. Mechanical properties

Mechanical properties of the majority of minerals that can be found in mudrocks have been studied, whereas organic matter properties are not well understood or investigated fully. This is mostly due to the restrictions on available equipment that are capable of measuring the moduli of organic matter. VKA (Visual Kerogen Assessment) of samples revealed the existence of various types of minerals along with the

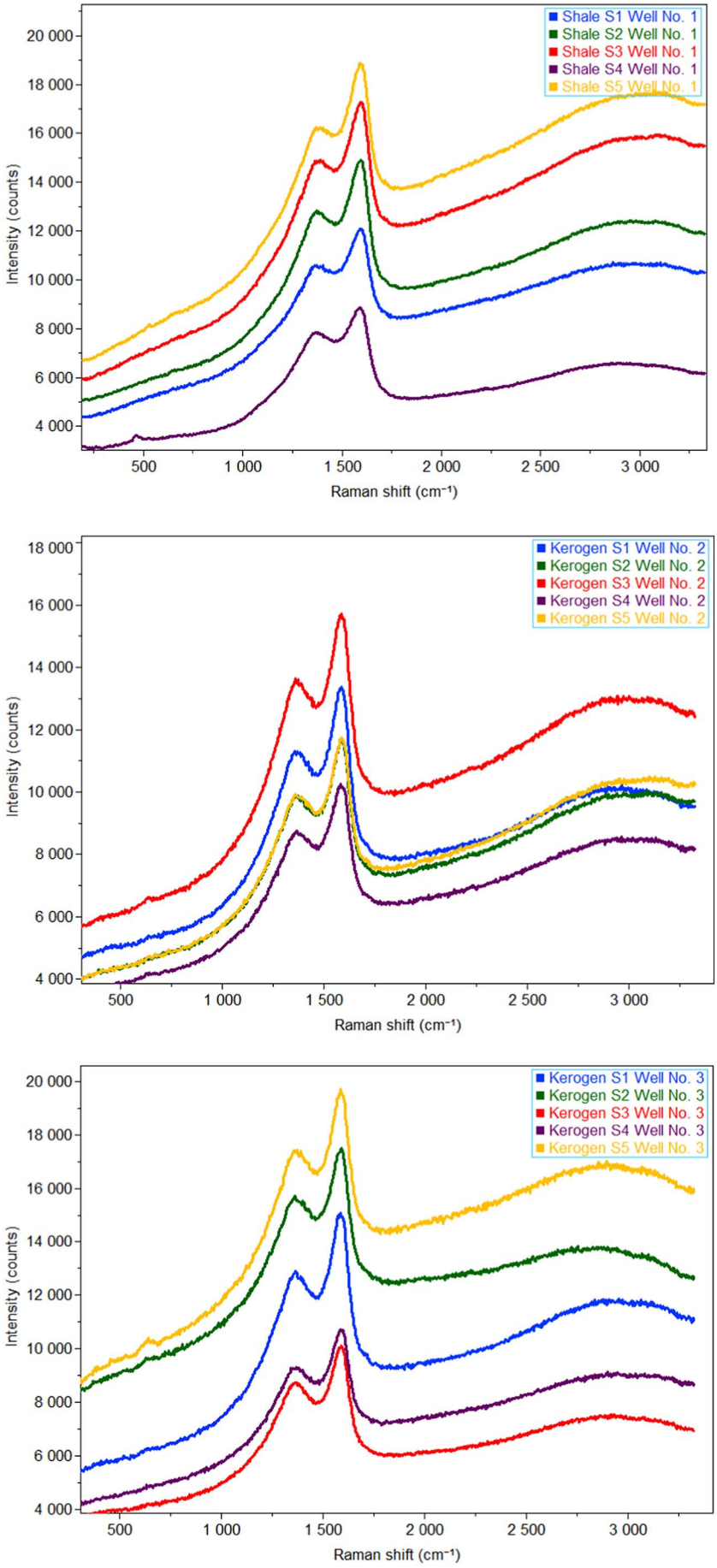

Fig. 7. Raman spectra (intensity versus Raman shift) for all samples with five time measurements on five spots.

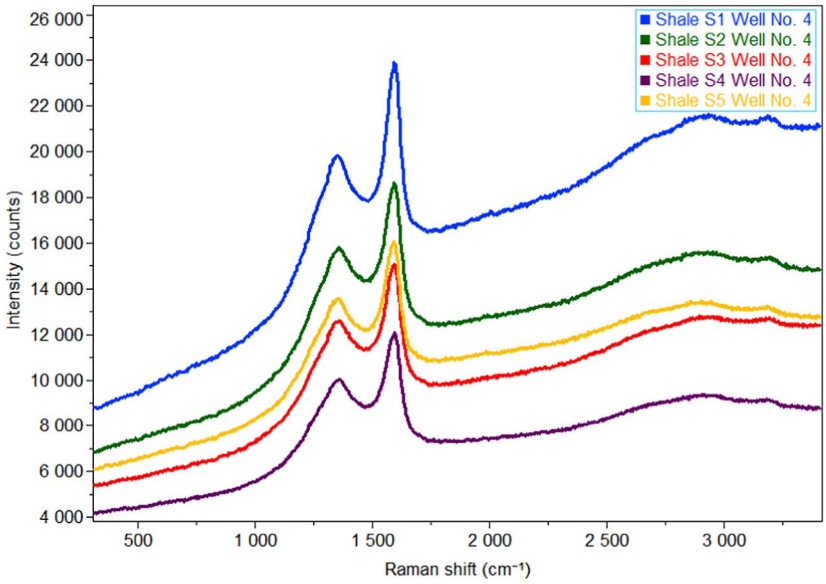

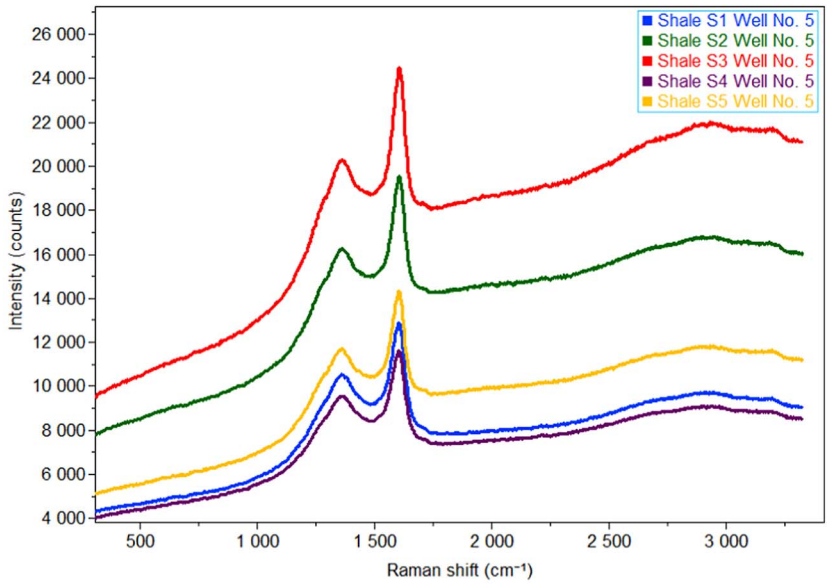

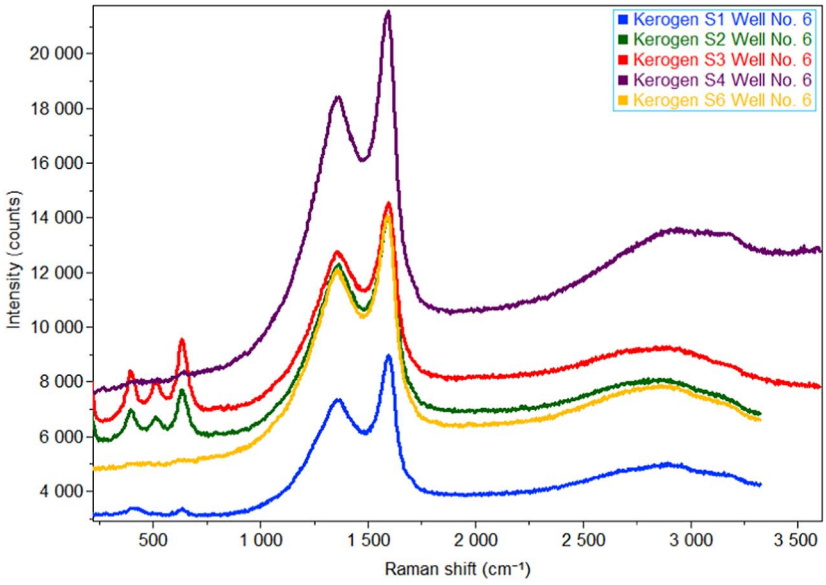

Fig. 7. (*continued*)

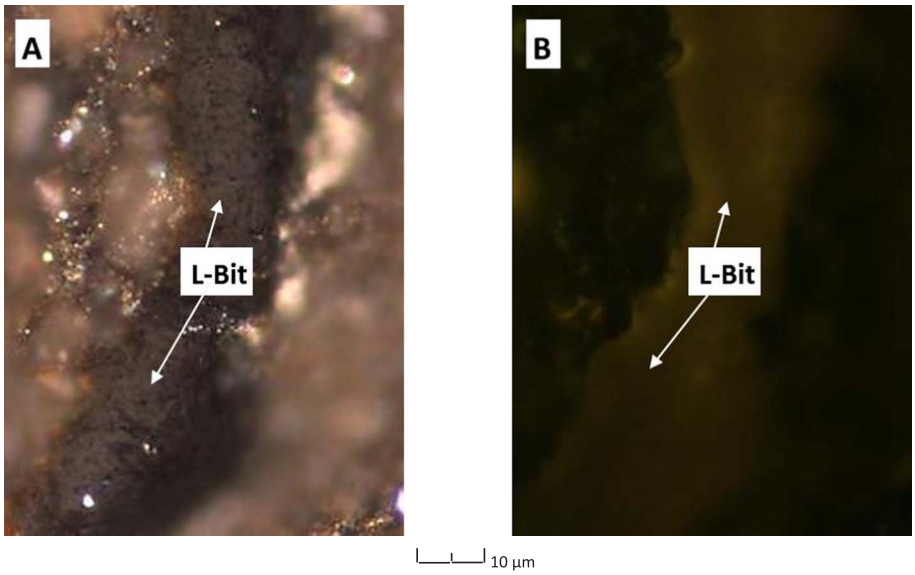

Fig. 8. (A) Hydrogen-rich low-reflecting bitumen (L-Bit) viewed under white reflected light. (B) The same view under UV light (fluorescence). Note the dull-yellow fluorescing of L-Bit. (For interpretation of the references to colour in this figure legend, the reader is referred to the web version of this article.)

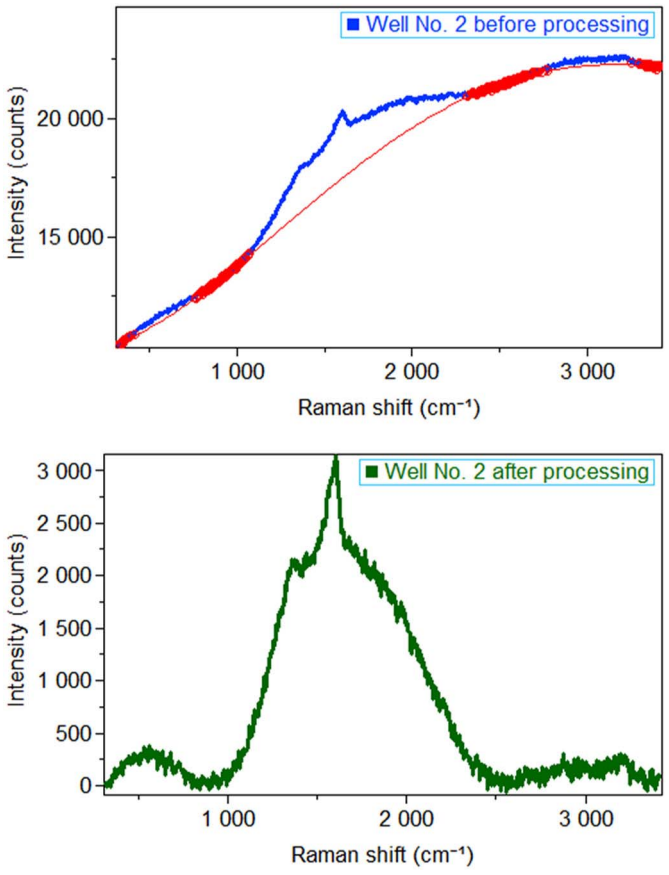

Fig. 9. Sample of Well No. 2: (top) before and (down) after processing by Labspec 6. Baseline subtraction method was used to have a better spectrum for determining band position. Polynomial baseline defined is shown in red, which was subtracted to yield a background free spectrum. (For interpretation of the references to colour in this figure legend, the reader is referred to the web version of this article.)

organic matter within the matrix, as seen in Fig. 11 from Well No. 4 and 6. It is found that clays followed by siliceous minerals and organic matter constitute the main portion of the sample weight. By comparing Young's modulus of kerogen, reported by Mavko et al. (2009), Kumar et al. (2012) and Eliyahu et al. (2015), with other inorganic parts that exist in mudrocks, it can be inferred that kerogen is the least stiff constituent component, Fig. 12.

Most of the attempts for studying in situ mechanical properties of shale have been made by nanoindentation (Zeszotarski et al., 2004; Ulm and Abousleiman, 2006; Bobko and Ulm, 2008; Ahmadov et al., 2008; Kumar et al., 2012; Shukla et al., 2013; Zargari et al., 2011). Nanoindentation mostly measures the micron- scale properties rather than true nano-scale ones. In this study, elastic modulus of organic matter was measured by the PeakForce Quantitative Nano-mechanical Mapping (QNM) mode of AFM. PeakForce QNM visualizes, identifies, and maps the elastic properties for every component separately in nanoscale. In this mode of AFM, the tip of the probe is pushed towards the surface of the sample until the PeakForce set point is reached (Li et al., 2017). Then it is withdrawn at the maximum adhesion point. While the probe scanning the surface of the sample, the deflection of the cantilever is measured. The deflection produces a Force-Distance curve which elastic modulus of matter can be calculated from. The details of the measurement technique can be found in the manuscript by Li et al. (2017). The measured Young's modulus for in-situ kerogen for our samples is reported in Table 3.

4. Results and discussion

Raman response shows that a trend exists between the depth of the samples and band position (Schito et al., 2017). Fig. 13 shows a decrease of D band positions with depth, from 1367 cm^{-1} to 1354 cm^{-1}, while there is no definitive relationship for G band positions with depth, which varies between 1591 cm^{-1} and 1600 cm^{-1}. Consequently, band separation depicts an increase with depth from 226 cm^{-1} to 243 cm^{-1}. Such trends are attributed to an increase in thermal maturity versus depth. As discussed earlier, previous Raman studies have documented systematic changes in band positions and separation in the Raman spectra for carbonaceous materials as a function of thermal maturity.

It was found that in response to an increase of thermal maturity, a shift in the position of the D band towards lower wavelength would take place, Fig. 14(A). This shift is attributed to the increase of larger aromatic clusters and more ordered-structure kerogen (Schito et al., 2017). We were not able to distinguish a similar trend for G band position, Fig. 14(B). Such observations are in agreement with those made in earlier studies (Ferrari and Robertson, 2000; Quirico et al., 2005;

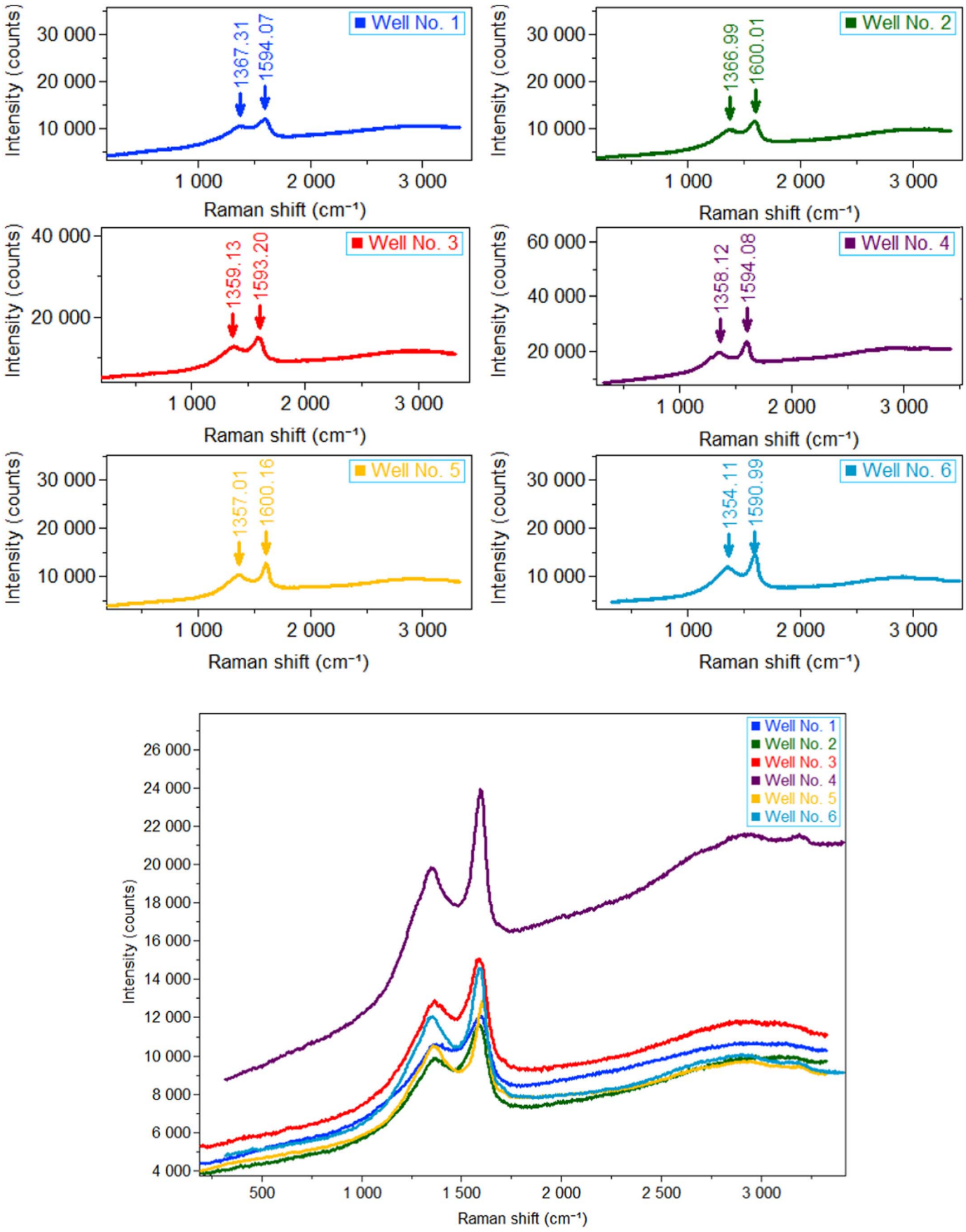

Fig. 10. (top) Mean of five time measurements of Raman spectra of each sample, (bottom) the same data, but spectra are overlaid in one plot for better comparison of band positions.

Table 2
Bands position of each well.

Well No.	D band (cm^{-1})	G band (cm^{-1})	G-D (cm^{-1})
1	1367.44	1594.09	226.65
2	1367.03	1600.02	232.99
3	1359.21	1593.25	234.04
4	1357.96	1594.03	236.07
5	1356.98	1600.30	243.32
6	1354.01	1590.96	236.95

Guedes et al., 2010). Statistical analysis shows that a logarithmic relationship (R^2 = 74%) exists between the band separation and %VRo for 11 different data sets including the one from the Bakken from this study, Fig. 14(C). The increase of the band separation with maturity can be referred to the shift in the D band position towards lower wavenumbers without any systematic change in the G band position. At initial stages of maturation, band separation increases with a higher intensity while this rapid growth tapers off over higher maturities. The same trend was found in coal where metamorphism concurrent to maturity at catagenesis happens faster than the metagenesis stage (for both fresh and laboratory matured coal observed by Kelemen and Fang, 2001). Moreover, Raman response can be also related to T_{max}, which is a thermal maturity index, Fig. 14(D).

It is believed that in immature source rock samples, the organic matter appears to surround other minerals, becoming a load-bearing part of the rock framework. However, as the maturity increases, kerogen becomes more isolated among other grains (Zargari et al., 2011; Zargari et al, 2015; Dietrich, 2015) and its Young's modulus increases. Few studies have been able to confirm this interpretation by direct measurement (Emmanuel et al., 2016; Li et al., 2017). In general, comparing %VRo with the measured Young's modulus for the samples in this study, it can be deduced when maturity increases from 0.38% to

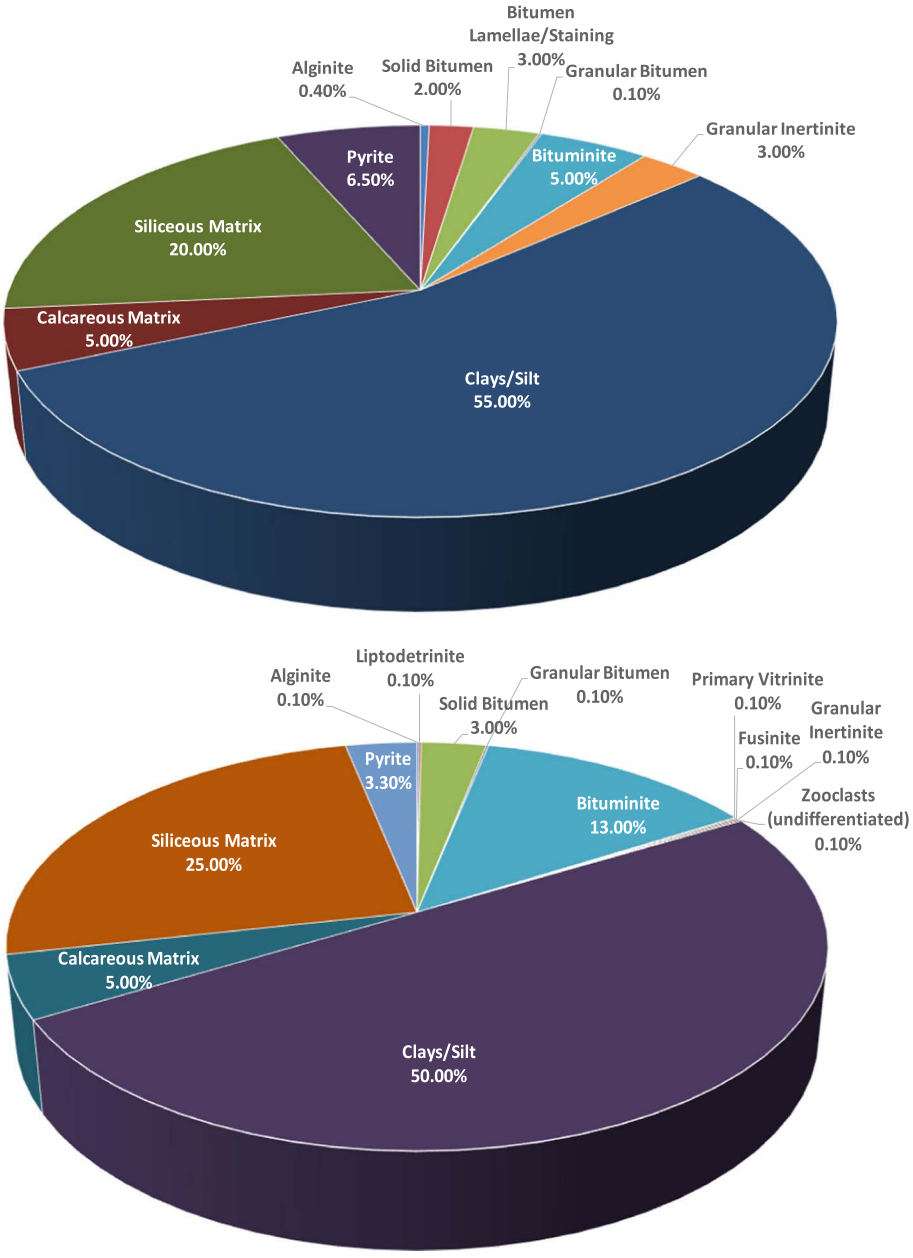

Fig. 11. Visual kerogen assessment on whole-rock sample was performed and the mineral percentage based on visual analysis are approximated for Well No. 4 (top) and Well No. 6 (down).

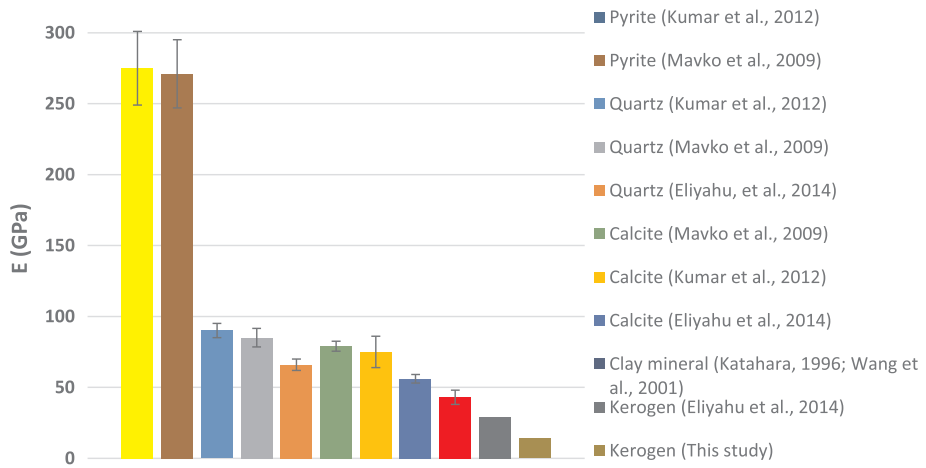

Fig. 12. Young's modulus of some sedimentary rock forming minerals. As it can be seen, kerogen is the least stiff constituent.

Table 3
Measured Young's modulus for in-situ kerogens in this study.

Well no.	E (GPa)
1	2.5
2	4
3	[a]
4	4.2
5	16
6	5.35

[a] Well No. 3 lacks Young's modulus measurement.

0.94% of %Ro, Young's modulus of corresponding samples increases from 2.5 GPa to 16 GPa. This phenomenon can be discussed from a molecular point of view. When maturity happens, kerogen loses heteroatoms (N, S, and O) and its aliphatic carbons (hydrogen-rich groups). The residue is a hydrogen-poor structure molecule, which is dominated by aromatic carbons. During the process of maturation, which increases with burial depth, pore-walls rupture. This sequence promotes the mechanical reorientation and alignment of the aromatic units, thus will facilitate the reduction of defects. This is due to diffusion, elimination of bonding vacancies and annealing of aromatic sheets to triperiodic graphite (Bustin, 1996). Therefore, from the early stages of maturation, the macromolecule arrangements transform gradually from the chaotic and mixed layers to a more ordered arrangement (Pan et al., 2013).

The previously mentioned interpretation is also consistent with observations by Quirico et al. (2005). They analyzed a few samples by high-resolution transmission electronic microscope (TEM), Fig. 15. TEM showed, in the samples with lower maturity, layers are stacked together in groups of two or three with length not > 1 nm. While, in the more mature samples, not only the number of stacked layers slightly increases but also the length of distorted layers reaches 4 nm (Quirico et al., 2005). Consequently, an increase in thermal maturity leads to a significant change in the molecular structure of kerogen (Emmanuel et al., 2016). This change can easily become apparent in Raman response. Considering the relationship that exists between maturity and Raman spectra and also the alliance between maturity with Young's modulus, Raman data can be used as an indirect method to study the mechanical properties of organic matter with high accuracy.

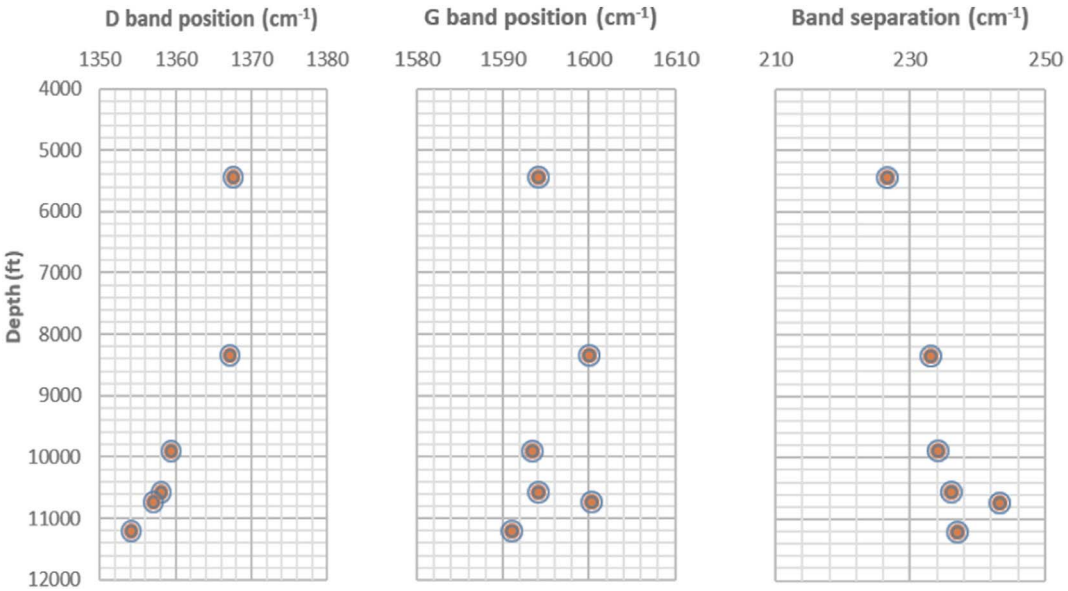

Fig. 13. (left) D band changes with depth, (middle) G band changes with depth, (right) band separation changes with depth. As seen, D band shows a decrease, G band no trends and band separation shows an increase with increasing depth.

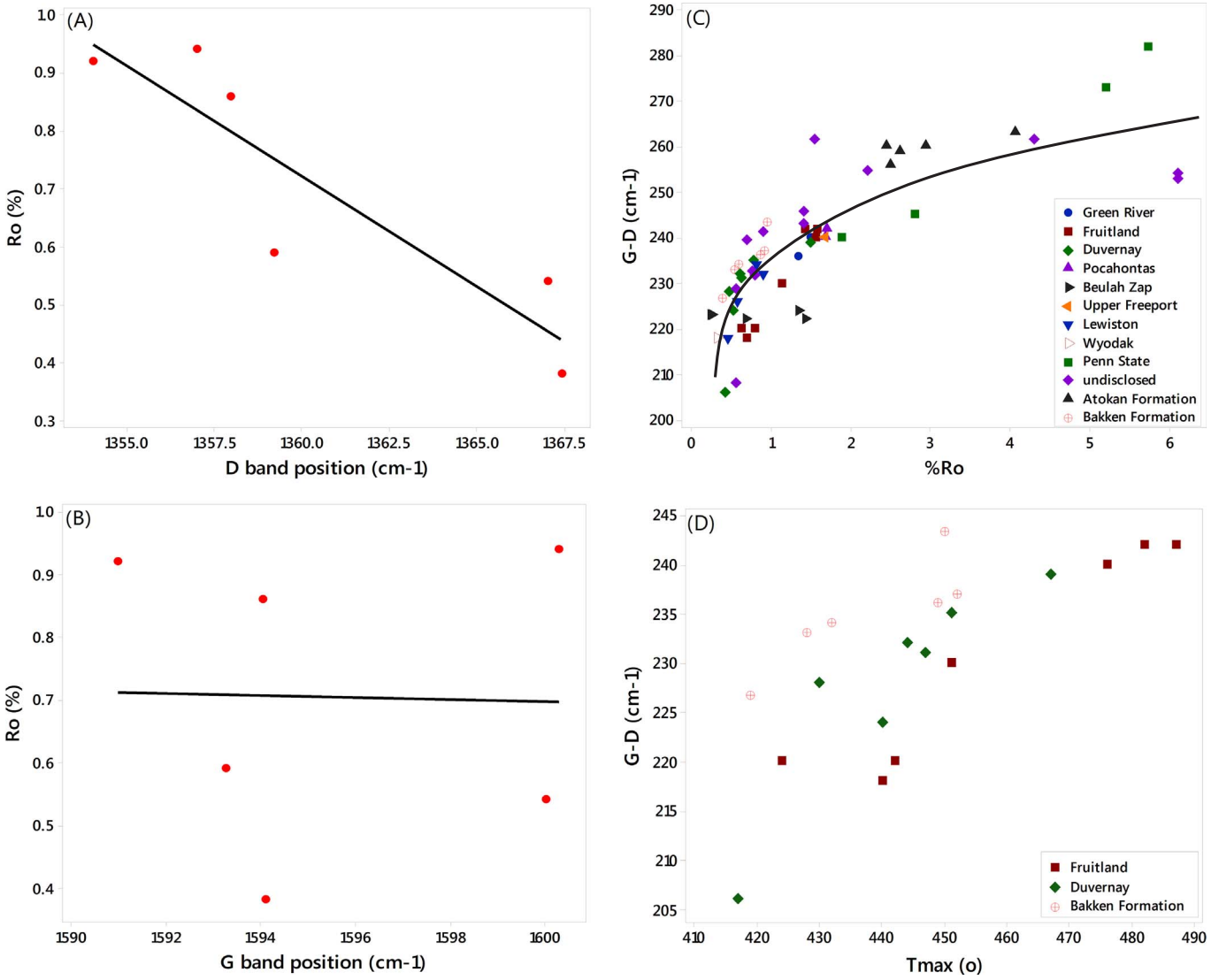

Fig. 14. (A) %Ro versus D band; (B) %Ro versus G band; (C) Band separation versus %Ro for 12 different data sets. There is a nonlinear relationship between Band separation and %Ro. Data are extracted from Spötl et al. (1998), Kelemen and Fang (2001), Sauerer et al. (2017) and results of this study; (D) T_{max} versus band separation for three different fields. Data are extracted from Sauerer et al. (2017) and results of this study. As seen, by increasing band separation, T_{max} is also increasing. It verifies Raman as a tool to predict thermal maturities in terms of vitrinite reflectance and Tmax from Rock-Eval.

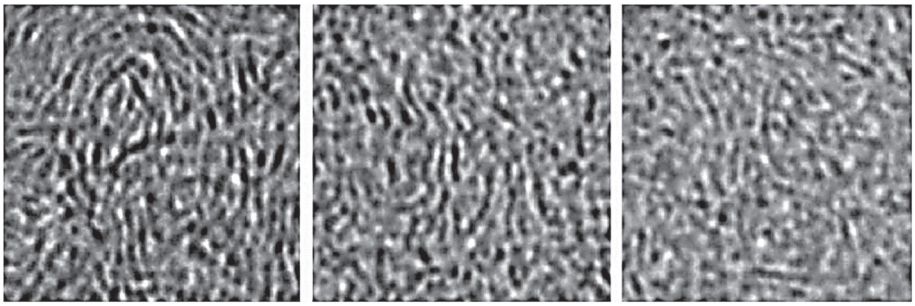

Fig. 15. Transmission electronic microscopy (TEM) image of three samples with different maturities. (Left) 7.5%VRo, (middle) 5.19%VRo, (right) 2.8%VRo. Changes in the molecular structure of kerogen at different maturity levels are visible.
Source: From Quirico et al., 2005.

Fig. 16 shows Young's modulus versus Raman responses for different samples. It can be seen that the band separation can be fitted to Young's modulus better with a nonlinear correlation, Fig. 14(B), compared to linear one, Fig. 14(A). This might be pertinent to the nonlinear correlation between %Ro and the band separation as shown in Fig. 14(C).

When %Ro varies from 0.3–3 (initial stages of maturation to late dry gas window), band separation varies approximately between 210 cm^{-1} to 255 cm^{-1}, respectively, Fig. 17. Based on non-linear correlation in Fig. 16(B), Young's modulus (E) can be estimated from 0.32 GPa to 40 GPa. This is in line with previous results by Eliyahu et al. (2015) who predicted E in the range of 0–25 GPa for maturities up to % Ro = 2.1, and Kumar et al. (2012), that presented E of 15–16 GPa for

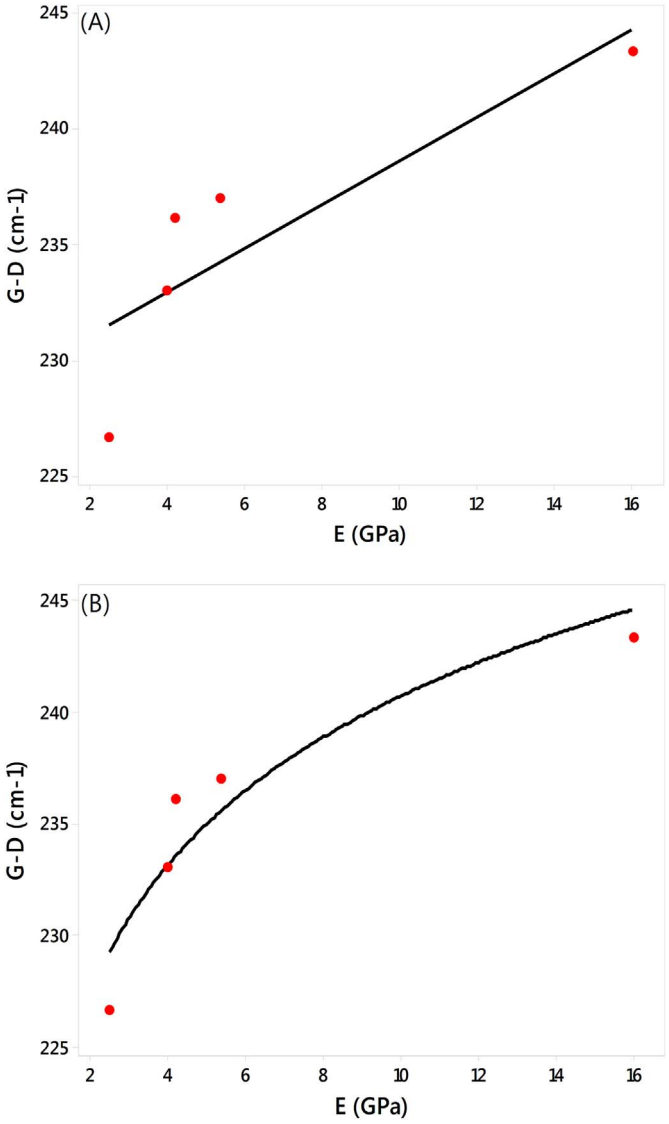

Fig. 16. (A) Young's modulus versus band separation with linear correlation with R^2 = 71%; (B) Young's modulus versus band separation with non-linear correlation with R^2 = 87%. As seen, non-linear correlation matches better with data which might be related to non-linear correlation between %Ro and band separation.

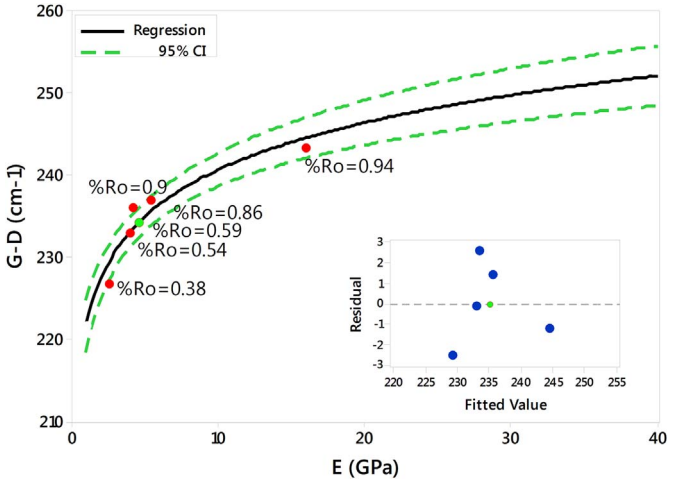

Fig. 18. Non-linear correlation between band separation and Young's modulus, with 95% confidence interval of regression and error profile. Predicted value for Well No.3 is shown in green dot. (For interpretation of the references to colour in this figure legend, the reader is referred to the web version of this article.)

higher maturity and 6–9 GPa for lower maturity samples in their study. Moreover, considering maturity of 2.1 (based on Eliyahu et al., 2015), Fig. 17 assigns corresponding band separation as almost 250 cm^{-1}. Fitted curve through the data from this study in Fig. 18 and extrapolated to higher values, predicts Young's modulus of around 25 GPa which is in line with what Eliyahu et al. (2015) measured.

Moreover, considering Table 3, the sample taken from Well No. 3 lacks Young's modulus measurement, whereas, Raman spectroscopy and maturity information are available. Having a band separation of 234 cm^{-1}, and using the curve in Fig. 18, Young's modulus of 4.11 GPa can be predicted for this sample. Considering %Ro of 0.59 for the sample, it should exhibit Young's modulus between the values that were measured for Well No. 2 and Well No. 4 (4 GPa and 4.2 GPa, respectively). Predicted E value for Well No. 3 is represented with a green dot in Fig. 18 and shows the accuracy of method.

The proposed method is a fast and non-destructive way to understand kerogen's modulus of elasticity by using Raman spectroscopy and considering its thermal maturity. High resolution for the laser focal volume of the Raman equipment allows for the analysis of small volumes of dispersed organic material with good precision. Furthermore,

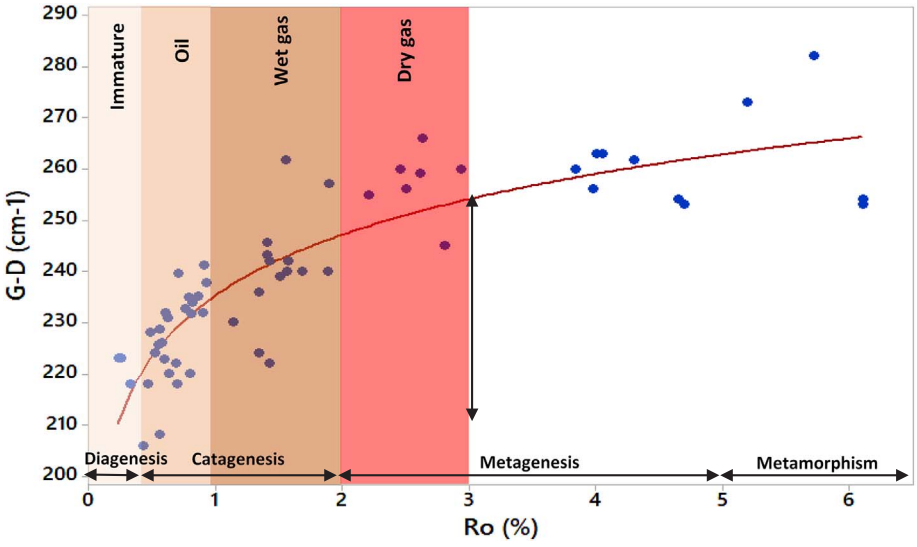

Fig. 17. Band separation versus maturity with general thermal maturity map overlaid. Considering %Ro = 3 as the late dry gas window, band separation of kerogen can vary from 210 to 255 cm^{-1}. Samples are the same as Fig. 13(C).

the minimal and rapid sample preparation for Raman spectroscopy enables us to evaluate both maturity and elastic properties of samples at the wellsite for real-time measurements. In future studies, the mechanical properties of more samples with higher thermal maturities are suggested.

5. Conclusion

In this study, we examined samples taken from the Upper and Lower members of the Bakken Formation from six different wells drilled in Williston Basin, ND. Rock-Eval 6 pyrolysis and optical microscopy analysis showed the presence of oil-prone Type II marine kerogen. Solid bitumen reflectance was used to determine the level of thermal maturity, which varied from immature to peak oil window. Raman spectroscopy was employed, as a potential indirect method, to predict the maturity and Young's modulus of the organic matter. Based on the results, the following conclusions were made:

- Raman spectroscopy, which is based on molecular vibrations, was able to detect molecular alterations in the organic matter as it undergoes changes in thermal maturity. Therefore, thermal maturity of the samples can be related to their Raman spectra.
- As maturity increases, major Raman signals start to separate from one another. This separation occurs between the G and D bands. The G band does not move significantly while the D band shifts towards lower wavelengths. From this observation, it is concluded that this specific Raman response directly correlates not only to the geochemical characteristics of the organic matter but also to the maturity of each sample.
- As thermal maturity increases, mechanical properties (e.g., elastic modulus) of organic matter alter. This alteration in elastic properties is due to macromolecular arrangements, transforming gradually from chaotic and mixed-layered to a better-ordered molecular structure.
- Comparing samples of different maturity levels to their corresponding predicted Young's moduli from Raman spectroscopy, it was observed that Young's modulus increases as maturity increases.
- Young's modulus was correlated to band separation by considering through a nonlinear relationship that takes into account the thermal maturity of the samples. However, we were not able to develop a robust connection between individual G and D band wavelengths with Young's modulus.
- Raman spectroscopy was able to estimate the Young's modulus of organic matter. It showed 0.32 GPa in the initial stages of maturation to 40 GPa in the late dry gas window.

To accomplish a more detailed analysis, we plan to extend this study by analyzing samples having a wide range of maturities and by incorporating minor Raman signals.

Funding

This research did not receive any specific grant from funding agencies in the public, commercial, or not-for-profit sectors.

Competing interest statement

There are no known competing interests.

References

Aghajanpour, A., Fallahzadeh, S.H., Khatibi, S., Hossain, M.M., Kadkhodaie, A., 2017. Full waveform acoustic data as an aid in reducing uncertainty of mud window design in the absence of leak-off test. J. Nat. Gas Sci. Eng. 45, 786–796.

Ahmadov, R., Vanorio, T., Mavko, G., 2008. Confocal Laser Scanning and Atomic-force Microscopy in Estimation of Elastic Properties of Organic-rich Rocks, Bazhenov Formation. AGU Fall Meeting Abstracts, Russia.

Alexeyev, A., Ostadhassan, M., Mohammed, R.A., Bubach, B., Khatibi, S., Li, C., Kong, L., 2017. Well Log Based Geomechanical and Petrophysical Analysis of the Bakken Formation.

Ammar, M., Galy, N., Rouzaud, J., Toulhoat, N., Vaudey, C., Simon, P., Moncoffre, N., 2015. Characterizing various types of defects in nuclear graphite using Raman scattering: heat treatment, ion irradiation and polishing. Carbon 95, 364–373.

Aoudia, K., Miskimins, J.L., Harris, N.B., Mnich, C.A., 2010. Statistical analysis of the effects of mineralogy on rock mechanical properties of the Woodford Shale and the associated impacts for hydraulic fracture treatment design. In: 44th US Rock Mechanics Symposium and 5th US-Canada Rock Mechanics Symposium. American Rock Mechanics Association.

Babaei, A., Ghanbari, A., Vakili-Tahami, F., 2015. Size-dependent behavior of functionally graded micro-beams, based on the modified couple stress theory. Thechnology 3, 364–372.

Babaei, A., Noorani, M.-R.S., Ghanbari, A., 2017. Temperature-dependent free vibration analysis of functionally graded micro-beams based on the modified couple stress theory. Microsyst. Technol. 1–12.

Behar, F., Beaumont, V., Penteado, H.D.B., 2001. Rock-Eval 6 technology: performances and developments. Oil Gas Sci. Technol. 56, 111–134.

Beyssac, O., Goffé, B., Chopin, C., Rouzaud, J., 2002. Raman spectra of carbonaceous material in metasediments: a new geothermometer. J. Metamorph. Geol. 20, 859–871.

Beyssac, O., Goffé, B., Petitet, J.-P., Froigneux, E., Moreau, M., Rouzaud, J.-N., 2003. On the characterization of disordered and heterogeneous carbonaceous materials by Raman spectroscopy. Spectrochim. Acta A Mol. Biomol. Spectrosc. 59, 2267–2276.

Bobko, C., Ulm, F.-J., 2008. The nano-mechanical morphology of shale. Mech. Mater. 40, 318–337.

Bustin, R., 1996. Mechanisms of graphite formation from kerogen: experimental evidence. In: Fuel and Energy Abstracts. Elsevier, pp. 187.

Cesare, B., Maineri, C., 1999. Fluid-present anatexis of metapelites at El Joyazo (SE Spain): constraints from Raman spectroscopy of graphite. Contrib. Mineral. Petrol. 135, 41–52.

Cheshire, S., Craddock, P.R., Xu, G., Sauerer, B., Pomerantz, A.E., McCormick, D., Abdallah, W., 2017. Assessing thermal maturity beyond the reaches of vitrinite reflectance and Rock-Eval pyrolysis: A case study from the Silurian Qusaiba formation. Int. J. Coal Geol. 180, 29–45.

Diessel, C., Brothers, R., Black, P., 1978. Coalification and graphitization in high-pressure schists in New Caledonia. Contrib. Mineral. Petrol. 68, 63–78.

Dietrich, A.B., 2015. The Impact of Organic Matter on Geomechanical Properties and Elastic Anisotropy in the Vaca Muerta Shale. Colorado School of Mines, Arthur Lakes Library.

Eliyahu, M., Emmanuel, S., Day-Stirrat, R.J., Macaulay, C.I., 2015. Mechanical properties of organic matter in shales mapped at the nanometer scale. Mar. Pet. Geol. 59, 294–304.

Emmanuel, S., Eliyahu, M., Day-Stirrat, R.J., Hofmann, R., Macaulay, C.I., 2016. Impact of thermal maturation on nano-scale elastic properties of organic matter in shales. Mar. Pet. Geol. 70, 175–184.

Espitalie, J., Deroo, G., Marquis, F., 1985. Rock-Eval pyrolysis and its applications. Rev. Inst. Francais Du Pet. 40, 563–579.

Ferralis, N., Matys, E.D., Knoll, A.H., Hallmann, C., Summons, R.E., 2016. Rapid, direct and non-destructive assessment of fossil organic matter via microRaman spectroscopy. Carbon 108, 440–449.

Ferrari, A.C., Robertson, J., 2000. Interpretation of Raman spectra of disordered and amorphous carbon. Phys. Rev. B 61, 14095.

Gerhard, L.C., Anderson, S.B., Fischer, D.W., 1990. Petroleum geology of the Williston Basin. AAPG Mem. 51, 507–559.

Ghanbari, A., Babaei, A., Vakili-Tahami, F., 2015. Free vibration analysis of micro beams based on the modified couple stress theory, using approximate methods. Technology 3, 136–143.

Gorbanenko, O.O., Ligouis, B., 2014. Changes in optical properties of liptinite macerals from early mature to post mature stage in Posidonia Shale (Lower Toarcian, NW Germany). Int. J. Coal Geol. 133, 47–59.

Guedes, A., Valentim, B., Prieto, A., Rodrigues, S., Noronha, F., 2010. Micro-Raman spectroscopy of collotelinite, fusinite and macrinite. Int. J. Coal Geol. 83, 415–422.

Guedes, A., Valentim, B., Prieto, A., Noronha, F., 2012. Raman spectroscopy of coal macerals and fluidized bed char morphotypes. Fuel 97, 443–449.

Hackley, P.C., Araujo, C.V., Borrego, A.G., Bouzinos, A., Cardott, B.J., Cook, A.C., Eble, C., Flores, D., Gentzis, T., Gonçalves, P.A., 2015. Standardization of reflectance measurements in dispersed organic matter: results of an exercise to improve interlaboratory agreement. Mar. Pet. Geol. 59, 22–34.

Hinrichs, R., Brown, M.T., Vasconcellos, M.A., Abrashev, M.V., Kalkreuth, W., 2014. Simple procedure for an estimation of the coal rank using micro-Raman spectroscopy. Int. J. Coal Geol. 136, 52–58.

Hu, R., Vernik, L., Nayvelt, L., Dicman, A., 2015. Seismic inversion for organic richness and fracture gradient in unconventional reservoirs: Eagle Ford Shale, Texas. Lead. Edge 34, 80–84.

Hutton, A., Bharati, S., Robl, T., 1994. Chemical and petrographic classification of kerogen/macerals. Energy Fuel 8, 1478–1488.

Kelemen, S., Fang, H., 2001. Maturity trends in Raman spectra from kerogen and coal. Energy Fuel 15, 653–658.

Keown, D.M., Li, X., Hayashi, J.-i., Li, C.-Z., 2007. Characterization of the structural features of char from the pyrolysis of cane trash using Fourier transform − Raman spectroscopy. Energy Fuel 21, 1816–1821.

Kuhn, P., Di Primio, R., Horsfield, B., 2010. Bulk Composition and Phase Behaviour of Petroleum Sourced by the Bakken Formation of the Williston Basin, Geological Society. Petroleum Geology Conference series. Geological Society of London, London,

pp. 1065–1077.
Kumar, V., Sondergeld, C.H., Rai, C.S., 2012. Nano to macro mechanical characterization of shale. In: SPE Annual Technical Conference and Exhibition. Society of Petroleum Engineers.
Lahfid, A., Beyssac, O., Deville, E., Negro, F., Chopin, C., Goffé, B., 2010. Evolution of the Raman spectrum of carbonaceous material in low-grade metasediments of the Glarus Alps (Switzerland). Terra Nova 22, 354–360.
LeFever, J.A., Martiniuk, C.D., Dancsok, E.F., Mahnic, P.A., 1991. Petroleum potential of the middle member, Bakken Formation, Williston Basin. In: Williston Basin Symposium.
Li, C., Ostadhassan, M., Kong, L., 2017. Nanochemo-mechanical Characterization of Organic Shale Through AFM and EDS, SEG Technical Program Expanded Abstracts 2017. Society of Exploration Geophysicists, pp. 3837–3840.
Liu, K., Ostadhassan, M., 2017. Microstructural and geomechanical analysis of Bakken shale at nanoscale. J. Pet. Sci. Eng. 153, 133–144.
Liu, K., Ostadhassan, M., Gentzis, T., Carvajal-Ortiz, H., Bubach, B., 2017. Characterization of geochemical properties and microstructures of the Bakken Shale in North Dakota. Int. J. Coal Geol.
Lünsdorf, N.K., 2016. Raman spectroscopy of dispersed vitrinite—Methodical aspects and correlation with reflectance. Int. J. Coal Geol. 153, 75–86.
Manjunath, G., Nair, R.R., 2015. Implications of the 3D micro scale coal characteristics along with Raman stress mapping of the scratch tracks. Int. J. Coal Geol. 141, 13–22.
Manjunath, G.L., Nair, R.R., 2017. Microscale assessment of 3D geomechanical structural characterization of gondawana shales. Int. J. Coal Geol. 181, 60–74.
Marshall, C.P., Edwards, H.G., Jehlicka, J., 2010. Understanding the application of Raman spectroscopy to the detection of traces of life. Astrobiology 10, 229–243.
Mason, J., Jordan, T., Carloni, J., Baker, S., Zehnder, A., 2014. Dependence of Micro-Mechanical Properties on Lithofacies: Indentation Experiments on Marcellus Shale, Unconventional Resources Technology Conference, Denver, Colorado, 25–27 August 2014. Society of Exploration Geophysicists, American Association of Petroleum Geologists, Society of Petroleum Engineers, pp. 1758–1770.
Mavko, G., Mukerji, T., Dvorkin, J., 2009. The Rock Physics Handbook: Tools for Seismic Analysis of Porous Media. Cambridge University Press.
Mumm, A.S., İnan, S., 2016. Microscale organic maturity determination of graptolites using Raman spectroscopy. Int. J. Coal Geol. 162, 96–107.
Pal-Bathija, A., Prasad, M., Liang, H., Upmanyu, M., Lu, N., Batzle, M., 2008. Elastic properties of clay minerals. In: SEG Technical Program Expanded Abstracts 2008. Society of Exploration Geophysicists, pp. 1610–1614.
Pan, J., Meng, Z., Hou, Q., Ju, Y., Cao, Y., 2013. Coal strength and Young's modulus related to coal rank, compressional velocity and maceral composition. J. Struct. Geol. 54, 129–135.
Peters, K., 1986. Guidelines for evaluating petroleum source rock using programmed pyrolysis. AAPG Bull. 70, 318–329.
Quirico, E., Rouzaud, J.-N., Bonal, L., Montagnac, G., 2005. Maturation grade of coals as revealed by Raman spectroscopy: Progress and problems. Spectrochim. Acta A Mol. Biomol. Spectrosc. 61, 2368–2377.
Reich, S., Thomsen, C., 2004. Raman spectroscopy of graphite. Philos. Transac. R. Soc. Lond. A 362, 2271–2288.
Sauerer, B., Craddock, P.R., AlJohani, M.D., Alsamadony, K.L., Abdallah, W., 2017. Fast and accurate shale maturity determination by Raman spectroscopy measurement with minimal sample preparation. Int. J. Coal Geol. 173, 150–157.
Schito, A., Romano, C., Corrado, S., Grigo, D., Poe, B., 2017. Diagenetic thermal evolution of organic matter by Raman spectroscopy. Org. Geochem. 106, 57–67.
Schön, P., Bagdi, K., Molnár, K., Markus, P., Pukánszky, B., Vancso, G.J., 2011. Quantitative mapping of elastic moduli at the nanoscale in phase separated polyurethanes by AFM. Eur. Polym. J. 47, 692–698.
Shukla, P., Kumar, V., Curtis, M., Sondergeld, C.H., Rai, C.S., 2013. Nanoindentation studies on shales. In: 47th US Rock Mechanics/Geomechanics Symposium. American Rock Mechanics Association.
Smith, M.G., Bustin, R.M., 1995. Sedimentology of the Late Devonian and Early Mississippian Bakken Formation, Williston Basin. In: Williston Basin Symposium.
Smith, M.G., Bustin, R.M., 2000. Late Devonian and Early Mississippian Bakken and Exshaw black shale source rocks, Western Canada Sedimentary Basin: a sequence stratigraphic interpretation. AAPG Bull. 84, 940–960.
Spötl, C., Houseknecht, D.W., Jaques, R.C., 1998. Kerogen maturation and incipient graphitization of hydrocarbon source rocks in the Arkoma Basin, Oklahoma and Arkansas: a combined petrographic and Raman spectrometric study. Org. Geochem. 28, 535–542.
Sweers, K., Van Der Werf, K., Bennink, M., Subramaniam, V., 2011. Nanomechanical properties of α-synuclein amyloid fibrils: a comparative study by nanoindentation, harmonic force microscopy, and Peakforce QNM. Nanoscale Res. Lett. 6, 270.
Tissot, B.P., Welte, D.H., 1984. Diagenesis, catagenesis and metagenesis of organic matter. In: Petroleum Formation and Occurrence. Springer, pp. 69–73.
Trtik, P., Kaufmann, J., Volz, U., 2012. On the use of peak-force tapping atomic force microscopy for quantification of the local elastic modulus in hardened cement paste. Cem. Concr. Res. 42, 215–221.
Tuinstra, F., Koenig, J.L., 1970. Raman spectrum of graphite. J. Chem. Phys. 53, 1126–1130.
Tuschel, D., 2013. Raman spectroscopy of oil shale. Spectroscopy 28, 5.
Tyson, R.V., 1995. Abundance of Organic Matter in Sediments: TOC, Hydrodynamic Equivalence, Dilution and Flux Effects, Sedimentary Organic Matter. Springer, pp. 81–118.
Ulm, F.-J., Abousleiman, Y., 2006. The nanogranular nature of shale. Acta Geotech. 1, 77–88.
Ulm, F.J., Vandamme, M., Bobko, C., Alberto Ortega, J., Tai, K., Ortiz, C., 2007. Statistical indentation techniques for hydrated nanocomposites: concrete, bone, and shale. J. Am. Ceram. Soc. 90, 2677–2692.
Wang, Y., Alsmeyer, D.C., McCreery, R.L., 1990. Raman spectroscopy of carbon materials: structural basis of observed spectra. Chem. Mater. 2, 557–563.
Waples, D.W., 1981. Organic Geochemistry for Exploration Geologists. Burgess Pub. Co.
Wilkins, R.W., Boudou, R., Sherwood, N., Xiao, X., 2014. Thermal maturity evaluation from inertinites by Raman spectroscopy: the 'RaMM' technique. Int. J. Coal Geol. 128, 143–152.
Wopenka, B., Pasteris, J.D., 1993. Structural characterization of kerogens to granulite-facies graphite: applicability of Raman microprobe spectroscopy. Am. Mineral. 78, 533–557.
Zargari, S., Prasad, M., Mba, K.C., Mattson, E., 2011. Organic maturity, hydrous pyrolysis, and elastic property in shales. In: Canadian Unconventional Resources Conference. Society of Petroleum Engineers.
Zargari, S., Canter, K.L., Prasad, M., 2015. Porosity evolution in oil-prone source rocks. Fuel 153, 110–117.
Zeszotarski, J.C., Chromik, R.R., Vinci, R.P., Messmer, M.C., Michels, R., Larsen, J.W., 2004. Imaging and mechanical property measurements of kerogen via nanoindentation. Geochim. Cosmochim. Acta 68, 4113–4119.
Zhao, Q., Wagner, H.D., 2004. Raman spectroscopy of carbon–nanotube–based composites. Philos. Transac. R. Soc. Lond. A 362, 2407–2424.
Zhao, Q., Frogley, M.D., Wagner, H.D., 2002. Direction-sensitive strain-mapping with carbon nanotube sensors. Compos. Sci. Technol. 62, 147–150.
Zhou, Q., Xiao, X., Pan, L., Tian, H., 2014. The relationship between micro-Raman spectral parameters and reflectance of solid bitumen. Int. J. Coal Geol. 121, 19–25.